IEEE Robotics and Automation Letters (RAL) paper presented at the
2020 IEEE/RSJ International Conference on Intelligent Robots and Systems (IROS)
October 25-29, 2020, Las Vegas, NV, USA (Virtual)

Combining Speed and Separation Monitoring with Power and Force Limiting for Safe Collaborative Robotics Applications

Niccolò Lucci, Bakir Lacevic, Andrea Maria Zanchettin, Paolo Rocco

Abstract— **Enabling humans and robots to safely work close to each other deserves careful consideration. With the publication of ISO/TS 15066 directives on this matter, two different strategies, namely the Speed and Separation Monitoring and the Power and Force Limiting, have been proposed. This paper proposes a method to efficiently combine the two aforementioned safety strategies for collaborative robotics operations. By exploiting the combination of the two, it is then possible to achieve higher levels of productivity, while still preserving safety of the human operators. This is achieved by the optimal scaling of the initially prescribed velocity, while preserving the path consistency of the robot trajectory. In a nutshell, the state of motion of each point of the robot is monitored so that at every time instant the robot is able to modulate its speed to eventually come into contact with a body region of the human, consistently with the corresponding biomechanical limit. Validation experiments have been conducted to establish that the proposed method enables substantially less stringent limits on robot performance while still allowing for the safety limits prescribed by ISO directives.**

I. Introduction

Collaborative robotics applications [1] are gaining attention in the robotics community, both from the academic and the industrial points of view. When it comes to allow robots to work in close proximity of the human operator, safety is an aspect of paramount importance, especially for the actual implementation of collaborative robotic applications in shopfloors, [2], [3]. This safety problem has been dealt with in several studies that take into consideration safety indexes as Head Injury Criteria (HIC) and study their dependence on robot parameters like mass or velocity (like [4] and [5] for example). According to the ISO/TS 15066, see [6], safety during collaborative operations can be guaranteed in mainly two ways: Speed and Separation Monitoring (SSM) and Power and Force Limiting (PFL). In short, SSM prescribes that the velocity of the robot must be related to the separating distance between the human and the robot itself so that at any time the robot actuation system has the necessary deceleration capability to achieve a complete stop before coming in contact with the worker. PFL, in turn, allows the robot to come into contact with the human worker with non-zero velocities, provided the amount of (kinetic) energy possibly transferred to the human does not exceed predefined thresholds. Notable results are reported for both the two strategies. The work in [7], later revised in [8], has been probably the first attempt in developing a control strategy for industrial robots satisfying the SSM requirement. In [9] a similar approach has been presented with the focus on formally guaranteeing the safety requirement. Marvel et al. in [10] completely address the problem, accounting for all possible factors influencing the robot behavior (payload, delayed reactions, etc.). Vogel et al. [11] approached the problem differently using a laser to project the safe space computed consistently with ISO/TS 15066. Byner et al. finally contributed in [12] with an industrial implementation with safety-rated distance monitoring sensors. The SSM criterion requires to monitor the worker position and thus implies the need for additional hardware. In turn, the PFL criterion does not necessarily need the adoption of additional hardware to monitor the workspace, as long as the velocity of the robot can be limited to safe values. Control strategies that explicitly account for the correlation between robot velocity and impact energy can be found in [13], [14]. As the key aspects of this kind of safety strategy are related to the reflected mass at the contact point, further investigation can be found in [15]. A more technological contribution to the implementation of PFL functionalities in a sensorless control strategy can be found in [16]. Finally, the work in [17] contributed to the biomechanical characterization of impacts as a function of the surface and the robot mechanical characteristics. The two safety criteria have different application scenarios. For example, PFL is suited when the human operator spends significant time in the workspace of the robot. In this case, the SSM would command the robot to be always still or to move very slowly, compromising productivity. In turn, for sporadic workspace sharing, the SSM criterion is surely recommended, allowing the robot to move at full speed when the operator is not present. On the other hand, a meaningful combination of PFL and SSM would arguably introduce substantial benefits in terms of productivity, particularly in tight collaboration scenarios requiring close and prolonged proximity between humans and robots. One of the first attempts to combine PFL and SSM strategies can be found in [18]. The approach therein, however, assumes a simplified spherical representation of human parts. Moreover the authors distinguish three separate working conditions: full speed, reduced speed and stop, which may turn out to be conservative since the dynamically varying speed is not fully enabled.

In this paper, we attempt to combine SSM and PFL safety strategies in a synergetic fashion. The proposed algorithm does not revolve around otherwise typical conservative

N. Lucci is with both Institute of Medical Robotics and Department of Automation, Shanghai Jiao Tong University, Shanghai, China and Politecnico di Milano niccolo.lucci@mail.polimi.it.

A.M. Zanchettin and P. Rocco are with Politecnico di Milano, Milano, Italy firstname.lastname@polimi.it.

B. Lacevic is with the University of Sarajevo, Sarajevo, Bosnia and Herzegovina bakir.lacevic@etf.unsa.ba.

assumptions on robots motion nor considerably simplified geometries. The main contributions of the paper are as follows.

- definition of a simple framework that combines SSM and PFL, enabling considerable improvements in productivity while preserving safety criteria;
- reduction of the problem onto an optimization algorithm that allows for a closed-form solution without any conservative assumptions;
- inclusion of the configuration-dependent inertial properties of the robot, which enables a more comprehensive treatment of safety constraints with respect to simply using the (typically considered) robot mass.

The remainder of this work is organized as follows. In Section II, a quick overview of background is given. Section III presents the approach developed in this work to combine the SSM and the PFL safety criteria. Based on the maximum velocity allowed by the combined criteria, a velocity scaling method is also proposed. Section IV describes the experimental setup and the implementation details, as well as the outcome of the experiments.

II. Background knowledge

Before proceeding further, a more detailed analysis of the two safety functionalities is needed. Letting v the (scalar approach) velocity of the robot, d the separating distance between the robot and the human, and T_s the stopping time, the SSM criterion prescribes that

$$v \leq \frac{d}{T_s} \tag{1}$$

In turn, the inequality established by the PFL criterion is the following one

$$|v| \leq \frac{F^{\max}}{\sqrt{k}} \sqrt{m_R^{-1} + m_H^{-1}} \tag{2}$$

where $F^{\max}$ represents the maximum contact force for specific body region, k stands for the effective spring constant for same body region, while m_R and m_H are the effective mass of the robot as a function of robot posture and motion and the effective mass of the human body region, respectively, [6].

For a generic robot having $m_R = 14\ kg$ and $T_s = 0.5\ s$, Fig. 1 shows the velocity limits corresponding to the SSM criterion and to the PFL criterion with respect to the upper arm (corresponding values for the quasi-static[1] case are $F^{\max} = 150\ N$, and $k = 30\ N/mm$, from [6]) of the human body. Here, the consideration of upper arm is arbitrary and just serves to provide an intuition behind the approach. Any other body part could be considered as well.

[1]A quasi-static contact between an operator and part of a robot system occurs when the operator body part can be clamped between a moving part of a robot system and another fixed or moving part of the robot cell. In this case the human reflected mass can be regarded as infinite, i.e. $m_H^{-1} \approx 0$. Note that by considering an infinite value for the mass of the human (clamped case), the upper limit for the admissible velocity decreases, thus making the analysis more conservative.

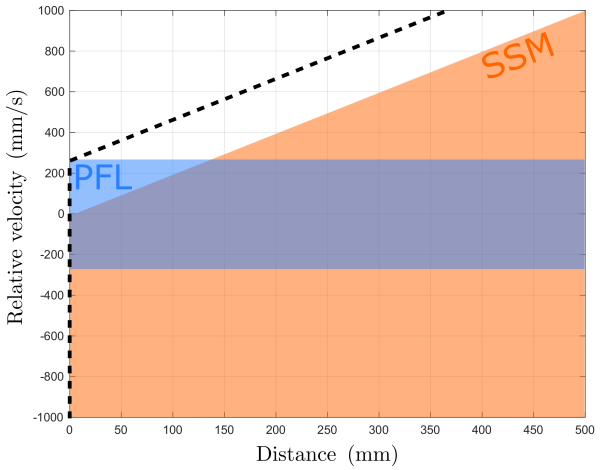

Fig. 1. Allowed velocity as a function of the separating distance for the SSM (orange) and PFL (blue) criteria. The dashed black line represents the combined criterion proposed in this paper.

As clearly visible in Fig. 1, there are situations, especially for reduced separating distances (under 130 mm referring to Fig. 1), where the PFL allows to move the robot with higher velocities than those allowed by the SSM. This is a straightforward consequence of the fact that, at small human-robot distances, the SSM would reduce the robots speed to a near zero values. In turn, as the PFL does not require a safety-rated sensing device to monitor the separating distance from the human, the SSM criterion can guarantee higher velocities when the human is far from the workspace of the robot, but also negative velocities, meaning that the robot can always move away from the human with any speed. In applications requiring sporadic, yet relatively long, workspace sharing between the human and the robot, relying solely on either the SSM or the PFL will inevitably lead to suboptimal performance.

This work addresses the problem of combining the two methodologies to improve productivity and to ensure the safety of the human worker. This way, if an actual collision between the human and the robot in motion cannot be avoided, the system will ensure that the speed of the robot at the impact would not lead to a severe injury for the human. The dashed black line in Fig. 1 indeed represents the maximum allowed velocity, as a function of the separating distance, with such a property. In other words, the robot is always capable of reducing its speed such that an unavoidable contact will ensure a tolerable energy transfer from the robot to the colliding body part. The final objective of this work is then to find such a curve for all the points of the robot and for all possible body parts of the human that might be involved in a contact.

III. Proposed approach

This section first describes the development of a novel safety requirements that combines SSM and PFL criteria. Inequalities corresponding to the dashed black line in Fig. 1 will be derived to account for the entire robot. In the

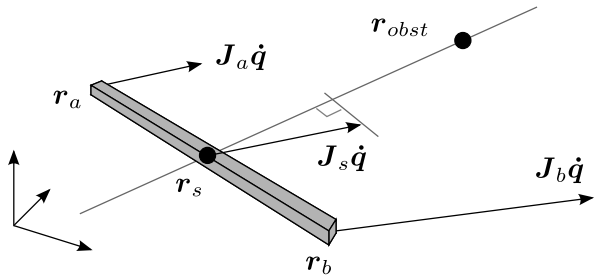

Fig. 2. Parameterisation for a beam (robot link) and for a point (obstacle).

second part, an algorithm to scale the robot velocity when not consistent with the safety requirements will be detailed.

A. Safety requirements

For quasi-static contacts, the safety criterion that combines the SSM and the PFL prescriptions can be expressed as follows

$$v \leq \frac{d}{T_s} + \frac{F^{\max}}{\sqrt{k}}\sqrt{m_R^{-1}} \tag{3}$$

and is represented by the dashed black line in Fig. 1. Notice that when a contact occurs, which happens for $d = 0$, the impact velocity is bounded from above by a quantity that satisfies the PFL criterion in (2). The presence of the maximum stopping time T_s, in turn, ensures that the robot has enough deceleration capabilities to eventually reach such a condition.

The given requirements can be further divided in two cases, one for positive distances, i.e. $d > 0$:

$$dv \leq d\left(\frac{d}{T_s} + \frac{F^{\max}}{\sqrt{k}}\sqrt{m_R^{-1}}\right), d > 0 \tag{4}$$

and one for situations close to a contact ($d \approx 0$):

$$v \leq \frac{F^{\max}}{\sqrt{k}}\sqrt{m_R^{-1}}, d \approx 0 \tag{5}$$

With the aim of applying the mentioned speed limit to the whole kinematic structure of the robot, consider a generic rigid link represented as a beam, as shown in Fig. 2. The position $\boldsymbol{r}_s$ and velocity $\boldsymbol{J}_s\dot{\boldsymbol{q}}$ (where $\boldsymbol{J_s}$ represents the positional Jacobian at the considered point s) of each point of the link can be written in terms of position and velocity of the two end points as follows:

$$\boldsymbol{r}_s = \boldsymbol{r}_a + s\left(\boldsymbol{r}_b - \boldsymbol{r}_a\right) \quad \boldsymbol{J}_s\dot{\boldsymbol{q}} = \boldsymbol{J}_a\dot{\boldsymbol{q}} + s\left(\boldsymbol{J}_b - \boldsymbol{J}_a\right)\dot{\boldsymbol{q}} \tag{6}$$

where $s \in [0, 1]$. Vectors $\boldsymbol{r}_a$ and $\boldsymbol{r}_b$ are the positions of the endpoints of the link, $\boldsymbol{J}_a$ and $\boldsymbol{J}_b$ are the related positional Jacobians, while $\dot{\boldsymbol{q}}$ stands for the vector of joint velocities. For a given point obstacle, detected at position $\boldsymbol{r}_{obst}$, define[2]

$$\boldsymbol{n} = \boldsymbol{r}_{os}/\|\boldsymbol{r}_{os}\|$$

the unit vector representing the direction from $\boldsymbol{r}_s$ to the point obstacle $\boldsymbol{r}_{obst}$. Then, the scalar approach velocity v is obtained as a projection of vector $\boldsymbol{v}_s = \boldsymbol{J}_s\dot{\boldsymbol{q}}$ onto vector $\boldsymbol{r}_{os}$, i.e., $v = \boldsymbol{v}_s^T\boldsymbol{n} = \dot{\boldsymbol{q}}^T\boldsymbol{J}_s^T\dfrac{\boldsymbol{r}_{os}}{\|\boldsymbol{r}_{os}\|}$. Furthermore, for the effective mass m_R of the robot at configuration $\boldsymbol{q}$, perceived at the operational point along a direction $\boldsymbol{n}$, the following holds [19]:

$$m_R^{-1} = \boldsymbol{n}^T\boldsymbol{J}_s\boldsymbol{B}^{-1}\boldsymbol{J}_s^T\boldsymbol{n}, \tag{7}$$

where $\boldsymbol{B}$ represents the configuration dependant robot inertia matrix. Using the fact that $d = \|\boldsymbol{r}_{os}\|$, the condition (4) may now be reformulated as:

$$\dot{\boldsymbol{q}}^T\boldsymbol{\beta}(s) \leq \frac{\|\boldsymbol{r}_{os}\|^2}{T_s} + C\sqrt{\boldsymbol{\beta}^T(s)\boldsymbol{B}^{-1}\boldsymbol{\beta}(s)}, \tag{8}$$

where $\boldsymbol{\beta}(s) = \boldsymbol{J}_s^T\boldsymbol{r}_{os}$ and $C = \frac{F^{\max}}{\sqrt{k}}$. Vector $\boldsymbol{\beta}(s)$ can be expressed as:

$$\boldsymbol{\beta}(s) = \left(\boldsymbol{J}_a^T + s\boldsymbol{J}_{ba}^T\right)\left(\boldsymbol{r}_{oa} - s\boldsymbol{r}_{ba}\right).$$

It has the same dimension as $\dot{\boldsymbol{q}}$ and $\boldsymbol{q}$ and can be roughly interpreted as a joint angular displacements required to bring the point $\boldsymbol{r}_s$ closer to $\boldsymbol{r}_{obst}$. Due to rigidity of the link, we have that $\left(\boldsymbol{J}_{ba}^T\boldsymbol{r}_{ba}\right)^T\dot{\boldsymbol{q}} = \boldsymbol{r}_{ba}^T\boldsymbol{J}_{ba}\dot{\boldsymbol{q}} = \boldsymbol{r}_{ba}^T\boldsymbol{v}_{ba} = 0$. Since this holds for an arbitrary joint velocity vector $\dot{\boldsymbol{q}}$, it implies that the vector $\boldsymbol{J}_{ba}^T\boldsymbol{r}_{ba}$ needs to be a zero vector. Thus, we have that:

$$\boldsymbol{\beta}(s) = \boldsymbol{y}_0 + \boldsymbol{y}_1 s,$$

where $\boldsymbol{y}_0 = \boldsymbol{J}_a^T\boldsymbol{r}_{oa}$ and $\boldsymbol{y}_1 = \boldsymbol{J}_{ba}^T\boldsymbol{r}_{oa} - \boldsymbol{J}_a^T\boldsymbol{r}_{ba}$. The left-hand side of (8) can now be expressed as:

$$\dot{\boldsymbol{q}}^T\boldsymbol{\beta}(s) = a_0 + a_1 s, \tag{9}$$

where $a_0 = \dot{\boldsymbol{q}}^T\boldsymbol{y}_0$, and $a_1 = \dot{\boldsymbol{q}}^T\boldsymbol{y}_1$.
Furthermore, the term $\|\boldsymbol{r}_{os}\|^2$ can be written as:

$$\begin{aligned}\|\boldsymbol{r}_{os}\|^2 &= \|\boldsymbol{r}_{obst} - \boldsymbol{r}_s\|^2 = \|\boldsymbol{r}_{oa} - s\boldsymbol{r}_{ba}\|^2 \\ &= \|\boldsymbol{r}_{oa}\|^2 - 2s\boldsymbol{r}_{oa}^T\boldsymbol{r}_{ba} + s^2\|\boldsymbol{r}_{ba}\|^2.\end{aligned} \tag{10}$$

Combining (9) and (10), we may write:

$$g(s, \dot{\boldsymbol{q}}) \equiv \dot{\boldsymbol{q}}^T\boldsymbol{\beta}(s) - \frac{\|\boldsymbol{r}_{os}\|^2}{T_s} = \alpha_2 s^2 + \alpha_1 s + \alpha_0, \tag{11}$$

where $\alpha_2 = -\|\boldsymbol{r}_{ba}\|^2/T_s$, $\alpha_1 = a_1 + 2\boldsymbol{r}_{oa}^T/T_s\boldsymbol{r}_{ba}$, $\alpha_0 = a_0 - \|\boldsymbol{r}_{oa}\|^2/T_s$. Now, the inequality (8) becomes:

$$g(s, \dot{\boldsymbol{q}}) \leq C\sqrt{\boldsymbol{\beta}^T(s)\boldsymbol{B}^{-1}\boldsymbol{\beta}(s)}. \tag{12}$$

The above inequality is irrational and hence it is recommended to discuss (for a given joint velocity vector $\dot{\boldsymbol{q}}$) the sign of the quadratic function $g(s, \dot{\boldsymbol{q}})$. In that regard, we identify three cases which are considered separately in the sequel.

1) $g(s, \dot{\boldsymbol{q}}) \leq 0,\ \forall s \in [0, 1]$,
2) $g(s, \dot{\boldsymbol{q}})$ changes its sign in $s \in [0, 1]$,
3) $g(s, \dot{\boldsymbol{q}}) \geq 0,\ \forall s \in [0, 1]$.

Due to the quadratic nature of $g(s, \dot{\boldsymbol{q}})$, it is straightforward to establish which of the above conditions hold. In case 1), the inequality (12) is clearly satisfied $\forall s \in [0, 1]$, meaning that the complete link is consistent with the safety criteria. If

[2]The following shortened symbols will be used in the following: $\boldsymbol{J}_{ba} = \boldsymbol{J}_b - \boldsymbol{J}_a$, $\boldsymbol{r}_{ba} = \boldsymbol{r}_b - \boldsymbol{r}_a$, $\boldsymbol{r}_{os} = \boldsymbol{r}_{obst} - \boldsymbol{r}_s$, $\boldsymbol{r}_{oa} = \boldsymbol{r}_{obst} - \boldsymbol{r}_a$.

$g(s,\dot{\boldsymbol{q}})$ changes its sign in $s \in [0,1]$ (case 2)), this implies that some parts of the link are guaranteed to be consistent with the safety criteria (the parts where $g(s,\dot{\boldsymbol{q}}) \leq 0$), while others need to be further investigated. Since $\alpha_2 < 0$, there can be only one subsegment where $g(s,\dot{\boldsymbol{q}}) > 0$ (see Fig. 3). This subsegment corresponds to a connected subset of the manipulator link that can clearly be analyzed within the case 3). It is necessary though, that this "truncated" link gets reparameterized, meaning that endpoint positions $\boldsymbol{r}_a$ and $\boldsymbol{r}_b$ get reassigned. Finally, under assumption that $g(s,\dot{\boldsymbol{q}}) \geq 0,\ \forall s \in [0,1]$, (12) is equivalent to:

$$g^2(s,\dot{\boldsymbol{q}}) \leq C^2 \boldsymbol{\beta}^T(s) \boldsymbol{B}^{-1} \boldsymbol{\beta}(s). \tag{13}$$

Using the expressions for $g^2(s,\dot{\boldsymbol{q}})$ and $\boldsymbol{\beta}(s)$, (13) can be written as:

$$\left(\alpha_2 s^2 + \alpha_1 s + \alpha_0\right)^2 \leq C^2 \left(\boldsymbol{y}_0^T + \boldsymbol{y}_1^T s\right) \boldsymbol{B}^{-1} \left(\boldsymbol{y}_0 + \boldsymbol{y}_1 s\right),$$

which is a quartic inequality in terms of parameter s:

$$f(s,\dot{\boldsymbol{q}}) \equiv \gamma_4 s^4 + \gamma_3 s^3 + \gamma_2 s^2 + \gamma_1 s + \alpha_0 \geq 0, \tag{14}$$

where

$$\gamma_4 = -\frac{\alpha_2^2}{C^2},\ \ \gamma_3 = -2\frac{\alpha_1 \alpha_2}{C^2},$$

$$\gamma_2 = \boldsymbol{y}_1^T \boldsymbol{B}^{-1} \boldsymbol{y}_1 - 2\frac{\alpha_1^2 + \alpha_0 \alpha_2}{C^2},$$

$$\gamma_1 = 2\boldsymbol{y}_0^T \boldsymbol{B}^{-1} \boldsymbol{y}_1 - 2\frac{\alpha_0 \alpha_1}{C^2},\ \ \gamma_0 = \boldsymbol{y}_0^T \boldsymbol{B}^{-1} \boldsymbol{y}_0 - \frac{\alpha_0^2}{C^2}.$$

To establish whether inequality (14) is satisfied $\forall s \in [0,1]$, it is sufficient to check the following condition:

$$f_{\min}(\dot{\boldsymbol{q}}) \equiv \min_{s \in [0,1]} f(s,\dot{\boldsymbol{q}}) \geq 0. \tag{15}$$

To compute the minimum $f_{\min}$ of the function $f(s,\dot{\boldsymbol{q}})$, having in mind that $f(s,\dot{\boldsymbol{q}})$ is smooth, it is sufficient to check the value of f at the boundary, i.e., $f(0)$ and $f(1)$, and at possible stationary points that belong to the interval $[0,1]$. More precisely:

$$f_{\min}(\dot{\boldsymbol{q}}) = \min_{s \in \mathcal{M}} f(s,\dot{\boldsymbol{q}}), \tag{16}$$

where the set $\mathcal{M} = \{0,1\} \cup \mathcal{SP}$, and $\mathcal{SP} = \left\{ s \in [0,1] \mid \frac{\partial f(s,\dot{\boldsymbol{q}})}{\partial s} = 0 \right\}$. The problem of computing the set $\mathcal{SP}$ is reduced to finding possible real roots $s \in [0,1]$ of the equation:

$$\frac{\partial f(s,\dot{\boldsymbol{q}})}{\partial s} = 4\gamma_4 s^3 + 3\gamma_3 s^2 + 3\gamma_2 s + \gamma_1 = 0. \tag{17}$$

This can be done by using some of the efficient linear-algebra-based solvers for polynomial equations, or even in closed form using Cardano formula.

Finally, the case of $d \approx 0$, i.e. the pure PFL criterion in (5) to be applied in very closed proximity, can be handled by requiring $\|\boldsymbol{J}_s \dot{\boldsymbol{q}}\| \leq C\sqrt{m_R^{-1}}$ for all points belonging to the link, hence for all $s \in [0,1]$. Since, from the triangular inequality we have that $\|\boldsymbol{J}_a \dot{\boldsymbol{q}} + s\boldsymbol{J}_{ba} \dot{\boldsymbol{q}}\| \leq \|\boldsymbol{J}_a \dot{\boldsymbol{q}}\| + s\|\boldsymbol{J}_{ba} \dot{\boldsymbol{q}}\|$ and the left-hand side term is linear with respect to s, we just need to require $\|\boldsymbol{J}_a \dot{\boldsymbol{q}}\| + \|\boldsymbol{J}_{ba} \dot{\boldsymbol{q}}\| \leq C\sqrt{m_R^{-1}}$ to be satisfied.

B. Trajectory scaling

If the safety requirements are satisfied for given nominal joint velocity $\dot{\boldsymbol{q}} = \dot{\boldsymbol{q}}_n$, obstacle position $\boldsymbol{r}_{obst}$, and robot link with endpoints $\boldsymbol{r}_a$ and $\boldsymbol{r}_b$, it is not necessary to scale the speed of trajectory. Otherwise, the problem is to find a maximal scaling coefficient $\delta \in [0,1]$ such that $\dot{\boldsymbol{q}} = \delta \dot{\boldsymbol{q}}_n$ implies that (12) is true for all $s \in [0,1]$. This consideration is clearly relevant only for case 3), remembering that case 2) can be reduced to case 3).

Assume the condition (15) is violated, meaning that $f_{\min}(\dot{\boldsymbol{q}}_n) < 0$. This implies that inequality (8) does not hold either. Thus, we can write:

$$\dot{\boldsymbol{q}}_n^T \boldsymbol{\beta}(s) = A(s) + m(s), \tag{18}$$

where $m(s) > 0$ and

$$A(s) = \frac{\|\boldsymbol{r}_{os}\|^2}{T_s} + C\sqrt{\boldsymbol{\beta}^T(s) \boldsymbol{B}^{-1} \boldsymbol{\beta}(s)}.$$

On the other hand, for the desired δ, we may impose the equality to hold, i.e.,

$$\delta \dot{\boldsymbol{q}}_n^T \boldsymbol{\beta}(s^*) = A(s^*), \tag{19}$$

where $s^* = \arg\min_{s \in [0,1]} f(s,\dot{\boldsymbol{q}}_n)$. Plugging $s = s^*$ in (18) and combining with (19), we have that:

$$\delta = \frac{A(s^*)}{A(s^*) + m(s^*)}. \tag{20}$$

Such obtained δ is then used to compute the candidate velocity vector $\dot{\boldsymbol{q}} = \delta \dot{\boldsymbol{q}}_n$, which is then checked for feasibility in the same fashion as $\dot{\boldsymbol{q}} = \dot{\boldsymbol{q}}_n$. The scaling may be repeated until δ converges. It appears that such procedure converges rapidly. In particular, the value of $m(s^*)$, which captures the degree to which the safety requirement is violated, reaches zero in finite number of iterations (usually 2-3). Unfortunately, we do not have a rigorous proof of convergence in finite time. However, such behavior can be explained as follows. If the slack variable $m(s^*)$ is large compared to $A(s^*)$, the scaling factor gets small, which implies a substantial decrease in the joint velocity that is now more likely to be consistent with the safety criterion. On the other hand, if the slack variable $m(s^*)$ is small compared to $A(s^*)$, the velocity is already close to satisfying the safety criterion, i.e., the procedure is close to convergence. The statistical analysis (based on slightly more than 106 runs of the procedure within a variety of simulated scenarios) shows that in about 62% of cases, the procedure converges after 2 iterations, in about 36% cases, the convergence occurs after 3 iterations, while $m(s^*)$ reaches zero value after 4 iterations in less than 2% of cases. Never have we observed that 5 or more iterations were needed for the convergence. The described procedure is condensed in Algorithm 1

Note that the combination of PFL and SSM requires a discussion of the sign of the quartic polynomial. On the other hand, either PFL or SSM strategy (if applied alone) would reduce to a discussion of a second order polynomial. The main contributor to the increase of the technical difficulty is

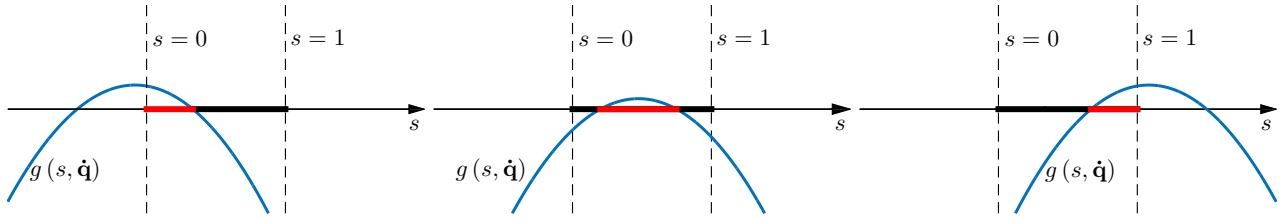

Fig. 3. Three cases that may occur when $g\left(s,\dot{\boldsymbol{q}}\right)$ changes sign in $s\in[0,1]$. In each scenario, the subset where $g\left(s,\dot{\boldsymbol{q}}\right)>0$ is connected (shown in red).

Algorithm 1 δ-SEARCH

$\delta \leftarrow 1$;
for $k=1$ **to** $k_{\max}$ **do**
  $\dot{\boldsymbol{q}} \leftarrow \delta\dot{\boldsymbol{q}}_n$;
  $s^* \leftarrow \arg\min_{s\in[0,1]} f\left(s,\dot{\boldsymbol{q}}\right)$;
  $A \leftarrow A\left(s^*\right)$;
  $\boldsymbol{\beta} \leftarrow \boldsymbol{\beta}\left(s^*\right)$;
  $m \leftarrow \dot{\boldsymbol{q}}^T\boldsymbol{\beta} - A$;
  if $m \leq 0$ **then**
    return δ
  $\delta \leftarrow \frac{A}{A+m}\delta$;
return δ

actually the reflected mass m_R defined in (7), which clearly implicitly appears in (8) as well. An easier approach would be to replace m_R with $M/2$ (M being the mass of the robot), which is the typical rough approximation of reflected mass [6]. However, neglecting the configuration- and motion-related dependencies of the robots inertial properties may conceal the possible room for performance improvement or, on the other hand, cause the safety constraints to be violated.

IV. Experimental validation

To verify and measure the benefit of the proposed approach, an experimental verification was carried out. Our mixed algorithm that combines SSM and PFL is conceived as an attempt to relax the constraints on robots velocity (and hence possibly increase the productivity) and make them more liberal with respect to SSM- or PFL-based constraints, when applied individually. This relaxation of constraints is carefully defined in order to preserve the safety criteria prescribed with the relevant standard. Mathematically, this corresponds to the fact that the right-hand-side (RHS) of the inequality (3) is larger than RHSs of inequalities (1) and (2). Therefore, our mixed approach is by construction set to outperform both SSM and PFL. Clearly, the interesting question is by how much? Arguably, it is difficult to assess the performance improvement in an analytical fashion since the amount by which the constraints are relaxed depends on many factors such as robots configuration, the environment setup, specific task, etc. Therefore, it is desirable to collect the empirical evidence via suitable experimental validation that covers a variety of scenarios, followed by statistical analysis of the appropriate performance metrics.

A. Experimental setup and implementation details

The experimental setup consists in a dual arm ABB YuMi robot, and a research version of the Smart Robots cognitive surveillance camera (see Fig. 4). The cognitive camera is responsible for tracking the position of the operator, who works in front of the robot, for evaluating the optimal speed scaling parameter δ in Algorithm 1, and for sending it to the robot through a standard Ethernet connection. At each time instant, the Smart Robots device performs the following processing steps:

1) retrieve the robot's configuration $\boldsymbol{q}$;
2) retrieve the point cloud of the environment;
3) classify the points of the 3D cloud in order to extract only those belonging to the human operator;
4) for each point, and based on the corresponding body part, evaluate $C = F^{\max}/\sqrt{k}$ according to the values reported in [6];
5) evaluate the maximum speed scaling parameter δ as in Algorithm 1, and sent it back to the robot.

While assigning the values of $C = F^{\max}/\sqrt{k}$ (step 4)), some considerations had to be addressed. In particular, the Yumi robot is already consistent with PFL constraints at full speed. Hence, there would be no point in implementing additional safety strategies to this robot. Therefore, the recommended values from [6] have been scaled down to the 10% of their nominal values, thus making the activation of the constraint possible. Roughly speaking, we artificially manipulate this constraint, only as a means to render the available robot relevant for the presented approach, by partially circumventing its inherent safety features. On the other hand, for an arbitrary robot that does not already have PFL embedded, the corresponding values do not need to be scaled. For instance, the UR5 robot is consistent with PFL at speed below 0.25m/s, though its full speed can reach 1m/s.

Clearly, the algorithm presented in Section III is being utilized within the step 5) of the above-described operation. Steps 1) - 4) serve to provide the algorithm with all the necessary inputs. It is worth pointing out that the optimization algorithm from Section III deals with the problem involving a single link and a single point obstacle. Therefore, the implementation of step 5) needs to loop the optimization algorithm over all the points from the corresponding cloud and over all the robots links. Note that this step also handles the computation of other quantities which play role in the algorithm described in Section III, such as: relevant positions

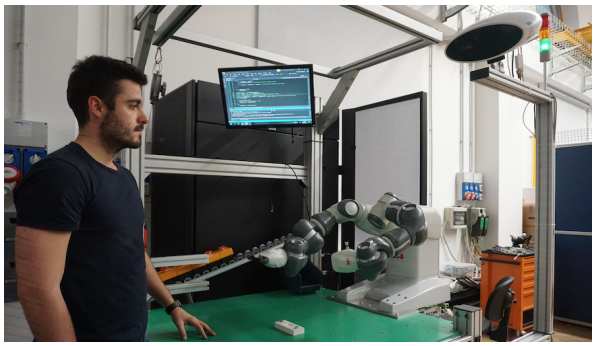

Fig. 4. Picture of the experimental setup consisting in a research SMART ROBOTS intelligent surveillance camera, and an ABB dual arm YUMI robot working in front of the operator.

$\boldsymbol{r}_a$, $\boldsymbol{r}_b$, Jacobians $\boldsymbol{J}_a, \boldsymbol{J}_b$ and configuration-dependent inertia matrix $\boldsymbol{B}$. Positions are clearly available from the forward kinematics, and so are the Jacobians. The inertia matrix $\boldsymbol{B}$, expressed as a function of $\boldsymbol{q}$, can be computed from the dynamic parameters of the robot, already available from CAD models or identifiable through experiments.

More in particular, the 3D camera embedded within the SMART ROBOTS device has a resolution of 512×424 pixels, while only approximately $2-3\%$ of them are used, being associated to the human operator. A $d^{\min} = 50\ mm$ threshold has been introduced to discriminate the two cases in (4) and (5). In fact, below this minimum distance, the camera, together with the developed algorithm, are no longer able to robustly discriminate between 3D points belonging to the human operator from those belonging to the robot or to the environment. For this reason, as already stated in Section III, a pure PFL method is applied in close vicinity.
The overall algorithm runs on the research version of the SMART ROBOTS embedded processing board (single core CPU, $2.1\ GHz$, with $8\ GB$ of memory) and takes approximately $120\ ms$ in the average case. Note that this time is absorbed by the inherent braking time. Moreover, this braking time may as well collect other constraints or requirements such as reaction times or additional distance margins.

The computational overhead introduced by the mixed approach, with respect to SSM, is the computation of extrema for the fourth-degree polynomial (which mainly reduces to finding the roots of a cubic equation) in comparison to computation of extrema for the second-degree polynomial. However, being available the exact solution to cubic equation (Cardano formula) or extremely efficient linear algebra libraries (e.g., Eigen3), the overhead is rendered negligible.

It is worth pointing out that the current implementation assumes that, in each cycle, the human is still, or at most slowly moving. While this may seem as a radical simplification, it does not jeopardize the generality of our approach. Nevertheless, our algorithm is perfectly capable of taking into account the motion of human parts. For instance, this problem has already been tackled in [20], where the initial human-occupied volume is augmented to account for the motion of the human within the robot stopping time. Such augmented volume is still represented via point cloud that can easily be used as an input to our algorithm. This is enabled by the fact that our algorithm is agnostic with respect to means by which the point cloud is generated.

B. Results and discussion

Several verification experiments have been run in order to test the validity of the approach, as well as to evaluate the performance of the mixed SSM and PFL safety criterion with respect to both PFL and SSM. In the following, the outcome of three experiments is reported to compare the three approaches. The experiments are performed in similar, yet not identical, conditions. The robot and the human operate in front of each other, sharing part of the workspace, as shown in Fig. 4. They both perform repetitive movements, within the shared workspace in all the three conditions. A metric, consistent in all the three scenarios, has been defined to objectively evaluate the performance of the implemented safety criteria. As the ultimate goal of the work developed in this paper is to maximise the velocity of the robot in performing its task, while still being safe with respect to the human operator, the robot velocity and the separating distance are the two main quantities of interest. It is worth mentioning that all the three safety criteria, the PFL, the SSM and the mixed SSM-PFL developed in this work, are all aligned with the safety regulations of the ISO/TS 15066 [6]. Therefore, to compare the three different approaches, a metrics that is uniquely associated with robot productivity has been introduced. Specifically, the ratio r between the scalar approach end-effector velocity in the direction of the closest point on the human body $\boldsymbol{n}^T\boldsymbol{J}_7\dot{\boldsymbol{q}}$ and the corresponding minimum separating distance $\min \boldsymbol{r}_{os}$ has been selected for the comparison. More formally $r = \boldsymbol{n}^T\boldsymbol{J}_7\dot{\boldsymbol{q}}/\min \boldsymbol{r}_{os}$. The higher this quantity, the faster the robot at the same separating distance. Only values with positive velocities, i.e. $\boldsymbol{n}^T\boldsymbol{J}_7\dot{\boldsymbol{q}} > 0$, and with a minimum separating distance $\min \boldsymbol{r}_{os}$ not higher than $400\ mm$ are considered, since from this point on, neither the SSM safety constraint nor the mixed safety constraint limit the robot velocity, thus they perform exactly the same. The negative approach velocities correspond to the cases when the robot moves away from the human and in these scenarios we do not expect our method to outperform SSM, though it will most likely outperform PFL. On the other hand, by taking into account the positive velocities only, we wanted to highlight potentially dangerous situations where our method has a clear advantage. Moreover, any improvement captured exclusively from motions directed at humans would clearly translate to general scenarios.

Unlike seemingly more intuitive choices for the proper metric such as task execution time, or maximum/average task velocity, the ratio r has several advantages. First, both the task time and the maximum/average task velocity are highly task-dependent. Thus, we would need to perform an extensive set of experiments to cover a wide variety of scenarios. Even in this case, the question remains whether some potentially relevant scenarios are neglected from con-

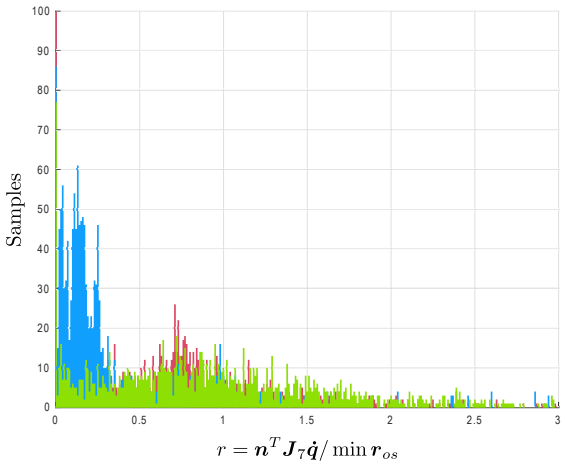

Fig. 5. Distribution of ratio r for the three scenarios: PFL (blue), SSM (red), and Mixed (green), sampled every 120 ms.

TABLE I

STATISTICAL COMPARISON BETWEEN THE PERFORMANCE INDICES

quantity	average	stdev	25-th	75-th	max
r_{PFL}	0.4526	0.7978	0.0890	0.3947	4.8702
r_{SSM}	0.6448	0.6354	0.0791	0.9261	4.9942
r_{Mixed}	1.1820	1.3981	0.4521	1.4517	18.464

sideration. Second, the ratio r enables a more efficient way of collecting the relevant data. Even a single experiment may provide a large number of values r, simply by computing it in each time cycle. Otherwise, we would need a dedicated experiment to compute a single value of the metric.

The collected values, for the three scenarios, are reported in Fig. 5 As one can notice, the average of r_{PFL} is clearly lower than the other two. Moreover, from Fig. 5 in particular we can state that our mixed algorithm performs better than the other two for medium and small distances since the right part of the graph is dominated by the green color. At the same time, we can also state that the Mixed algorithm performs the same as SSM for high distances (as stated previously, the robot reaches its maximum velocity without being limited for safety reasons neither by SSM nor by the Mixed one) since, in the middle part of the graph, the two superimpose. Furthermore, a complete statistical comparison is reported in Tab. I and shown in the box plots of Fig. 6. Statistical tests confirm that SSM outperform the PFL method (left tailed Mann-Whitney-Wilcoxon, $p = 1.39 \cdot 10^{-27}$), while the developed mixed approach outperforms SSM (left tailed Mann-Whitney-Wilcoxon, $p = 7.21 \cdot 10^{-54}$), in both cases with a very high statistical significance. Finally, for a further confirmation of the higher performance of the mixed SSM and PFL method developed in this work as compared to the two separate methods, Figures 7 and 8 report the distribution of the end-effector velocity $\boldsymbol{n}^T \boldsymbol{J}_7 \dot{\boldsymbol{q}}$ in the three considered scenarios (only positive values are reported). Also in this case SSM outperforms the PFL ($p = 5.65 \cdot 10^{-114}$), while, again, the mixed approach allows higher robot velocities with respect to the pure SSM criterion ($p = 6.46 \cdot 10^{-16}$). In terms

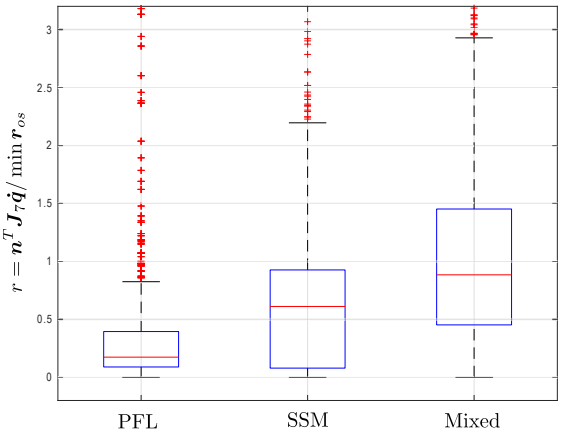

Fig. 6. Box plots of the three distributions of r_{PFL}, r_{SSM} and the proposed r_{Mixed}.

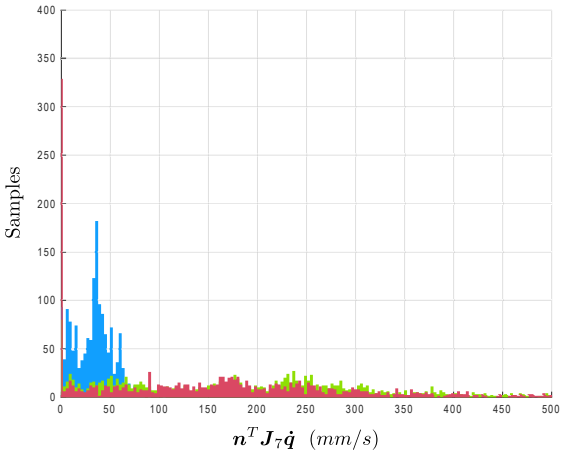

Fig. 7. Distribution of the end-effector approach velocity $\boldsymbol{n}^T \boldsymbol{J}_7 \dot{\boldsymbol{q}}$ for the three scenarios: PFL (blue), SSM (red), and Mixed (green), sampled every 120 ms.

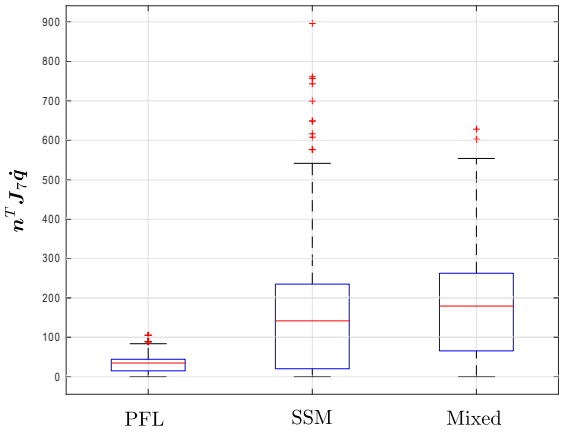

Fig. 8. Box plots of the three distributions of the end-effector velocity $\boldsymbol{n}^T \boldsymbol{J}_7 \dot{\boldsymbol{q}}$ for the three scenarios: PFL, SSM, and Mixed.

of end-effector velocity, on average, the mixed approach performs 20% better than SSM and 460% better than PFL.

Not surprisingly, both metrics used in the paper (the ratio r and the end-effector approach velocity $\boldsymbol{n}^T \boldsymbol{J}_7 \dot{\boldsymbol{q}}$)

indicated the substantial performance improvement of the mixed approach compared to PFL and SSM when applied separately. For instance, the ratio r for the mixed approach is on average almost twice as large with respect to SSM and even more when compared with PFL. Another expected behavior is that the improvement is more emphasized in scenarios involving tight collaboration, i.e., when the average human-robot distances are considerably small. The mixed approach performs pretty much the same as SSM for larger distances. This is not surprising since the robot may reach its maximum velocity without being limited for safety reasons neither by SSM nor by the mixed approach.

While the presented approach has shown to be promising for enhancing productivity in collaborative applications, it has two main limitations. The first one is related to a specific geometric representation of humans. The current version of the algorithm assumes that human operators are represented via point clouds. Such an approach is arguably less general than the surface-based representation, e.g., using triangle meshes. However, despite our best efforts, the optimization problem, which stems from the assumption of triangle-based obstacles, remains intractable. The second limitation of the methods scope is inherited from the potential limitations of the robot itself. Namely, the algorithm assumes that the robots design is consistent with the PFL paradigm. While in principle the algorithm can be applied to an arbitrarily articulated robot, the PFL-based assumption may exclude some robots that are not intended for collaboration, e.g., robots having sharp edges, operating heavy payloads, etc.

V. Conclusions

In this paper, a new strategy to scale the velocity of an industrial robot along a given path, so as to be consistent with ISO/TS 15066 safety standards, has been proposed. The method enforces a combination of the Speed and Separation Monitoring with the Power and Force Limiting criteria, reaching a higher overall production efficiency reaping full benefit of the possibility for collaborative robots to gently approach the human body in case of collisions, while avoiding unnecessary velocity limitations when they are not justified by the perceived distance between human and robot. The method selects the scaling coefficient in such a way that the prescriptions of the safety standards are rigorously satisfied for all points of the robot, at all time instants. The solution is amenable to easy implementation in a realistic industrial scenario, as the scaling factor can be conveniently assigned to the robot through an Ethernet connection, without requiring specific or research-oriented robot controller interfaces. A safety-rated device to perceive the distance between human and robot is required though.

Future work will explore the possibilities to enable more general geometric representations, both for humans and for robots links. Moreover, the motion of humans will be considered as well.

References

[1] A. Ajoudani, A. M. Zanchettin, S. Ivaldi, A. Albu-Schäffer, K. Kosuge, and O. Khatib, "Progress and prospects of the human–robot collaboration," *Autonomous Robots*, vol. 42, no. 5, pp. 957–975, 2018.

[2] S. Robla-Gómez, V. M. Becerra, J. R. Llata, E. Gonzalez-Sarabia, C. Torre-Ferrero, and J. Perez-Oria, "Working together: A review on safe human-robot collaboration in industrial environments," *IEEE Access*, vol. 5, pp. 26 754–26 773, 2017.

[3] P. A. Lasota, T. Fong, J. A. Shah *et al.*, "A survey of methods for safe human-robot interaction," *Foundations and Trends® in Robotics*, vol. 5, no. 4, pp. 261–349, 2017.

[4] S. Haddadin, A. Albu-Schäffer, and G. Hirzinger, "Safety evaluation of physical human-robot interaction via crash-testing." in *Robotics: Science and Systems*, vol. 3. Citeseer, 2007, pp. 217–224.

[5] S. Haddadin, A. Albu-Schaffer, and G. Hirzinger, "The role of the robot mass and velocity in physical human-robot interaction-part i: Non-constrained blunt impacts," in *2008 IEEE International Conference on Robotics and Automation*. IEEE, 2008, pp. 1331–1338.

[6] ISO TC184/SC2, *ISO/TS 15066 Robots and robotic devices – Safety requirements for industrial robots – Collaborative operation*, 2013.

[7] A. M. Zanchettin and P. Rocco, "Path-consistent safety in mixed human-robot collaborative manufacturing environments," in *2013 IEEE/RSJ International Conference on Intelligent Robots and Systems*. IEEE, 2013, pp. 1131–1136.

[8] A. M. Zanchettin, N. M. Ceriani, P. Rocco, H. Ding, and B. Matthias, "Safety in human-robot collaborative manufacturing environments: Metrics and control," *IEEE Transactions on Automation Science and Engineering*, vol. 13, no. 2, pp. 882–893, 2015.

[9] M. J. Zeestraten, A. Pereira, M. Althoff, and S. Calinon, "Online motion synthesis with minimal intervention control and formal safety guarantees," in *2016 IEEE International Conference on Systems, Man, and Cybernetics (SMC)*. IEEE, 2016, pp. 002 116–002 121.

[10] J. A. Marvel and R. Norcross, "Implementing speed and separation monitoring in collaborative robot workcells," *Robotics and computer-integrated manufacturing*, vol. 44, pp. 144–155, 2017.

[11] C. Vogel, C. Walter, and N. Elkmann, "Safeguarding and supporting future human-robot cooperative manufacturing processes by a projection-and camera-based technology," *Procedia Manufacturing*, vol. 11, pp. 39–46, 2017.

[12] C. Byner, B. Matthias, and H. Ding, "Dynamic speed and separation monitoring for collaborative robot applications–concepts and performance," *Robotics and Computer-Integrated Manufacturing*, vol. 58, pp. 239–252, 2019.

[13] R. Rossi, M. P. Polverini, A. M. Zanchettin, and P. Rocco, "A pre-collision control strategy for human-robot interaction based on dissipated energy in potential inelastic impacts," in *2015 IEEE/RSJ International Conference on Intelligent Robots and Systems (IROS)*. IEEE, 2015, pp. 26–31.

[14] A. Meguenani, V. Padois, and P. Bidaud, "Control of robots sharing their workspace with humans: an energetic approach to safety," in *2015 IEEE/RSJ International Conference on Intelligent Robots and Systems (IROS)*. IEEE, 2015, pp. 4678–4684.

[15] N. Mansfeld, B. Djellab, J. R. Veuthey, F. Beck, C. Ott, and S. Haddadin, "Improving the performance of biomechanically safe velocity control for redundant robots through reflected mass minimization," in *2017 IEEE/RSJ International Conference on Intelligent Robots and Systems (IROS)*. IEEE, 2017, pp. 5390–5397.

[16] K. Kokkalis, G. Michalos, P. Aivaliotis, and S. Makris, "An approach for implementing power and force limiting in sensorless industrial robots," *Procedia CIRP*, vol. 76, pp. 138–143, 2018.

[17] H. Shin, K. Seo, and S. Rhim, "Allowable maximum safe velocity control based on human-robot distance for collaborative robot," in *2018 15th International Conference on Ubiquitous Robots (UR)*. IEEE, 2018, pp. 401–405.

[18] P. Svarny, M. Tesar, J. K. Behrens, and M. Hoffmann, "Safe physical hri: Toward a unified treatment of speed and separation monitoring together with power and force limiting," in *2019 IEEE/RSJ International Conference on Intelligent Robots and Systems (IROS)*. IEEE, 2019.

[19] O. Khatib, "Inertial properties in robotic manipulation: An object-level framework," *The international journal of robotics research*, vol. 14, no. 1, pp. 19–36, 1995.

[20] M. Ragaglia, A. M. Zanchettin, and P. Rocco, "Trajectory generation algorithm for safe human-robot collaboration based on multiple depth sensor measurements," *Mechatronics*, vol. 55, pp. 267–281, 2018.